Sensors & Actuators: B. Chemical 394 (2023) 134350

Contents lists available at ScienceDirect

Sensors and Actuators: B. Chemical

journal homepage: www.elsevier.com/locate/snb

Highly stable and reversible hydrogen sensors using Pd-coated SnO_2 nanorods and an electrode–substrate interface as a parallel conduction channel

Jinkyo Jeong [a], Jung-Woo Lee [b,c], Jaeung Lee [d], Kyusik Shin [d], Hyun-Sook Lee [d,*], Wooyoung Lee [a,d,**]

[a] Department of Vehicle Convergence Engineering, Yonsei University, Seoul 03722, Republic of Korea
[b] KIURI Institute, Yonsei University, Seoul 03722, Republic of Korea
[c] Department of Materials Science and Engineering, Hongik University, Sejong 30016, Republic of Korea
[d] Department of Materials Science and Engineering, Yonsei University, Seoul 03722, Republic of Korea

ARTICLE INFO

Keywords:
Gas sensor
Hydrogen
SnO_2 nanorod
Schottky barrier
Dual-channel sensor

ABSTRACT

We demonstrated highly stable and reversible H_2 sensors using a dual electron-conduction channel comprising Pd-coated SnO_2 nanorods (NRs) and a parallel conduction channel containing Cr/native oxide/p-type Si interface. The dual-channel sensor exhibited highly reversible resistance changes during H_2 in-and-out cycles at operating temperatures of 25 °C– 100 °C, while typical single-channel sensors with SnO_2 NRs fabricated on SiO_2 (300 nm)/Si substrates showed irreversible response because of insufficient recovery from Pd-H_x to Pd-O_x. In particular, the sensor showed significantly high repeatability, long-term stability, and selectivity for H_2 sensing at 80 °C. Additionally, the time taken to detect H_2 above 1% was less than 2 s and the response to H_2 above 500 ppm was unaffected by high humidity. These results indicate that the dual-channel Pd-coated SnO_2 NR sensor is suitable for applications such as hydrogen leak detectors that require high speed and precision. Moreover, it was found that the sensor could detect H_2 below 0.5 ppm even at low temperatures. This work provides a pathway for improving gas-sensing performance by interface engineering, enabling various practical hydrogen sensor applications.

1. Introduction

Recently, hydrogen (H_2) has been highlighted as a source of future energy owing to the necessity of transition to green energy, which can achieve CO_2-free energy generation with high efficiency [1,2]. For example, fuel cell electric vehicles and residential fuel cells are systems that use H_2 energy by converting it into electrical energy [1,2]. Accordingly, the storage, transfer, and usage of H_2 gas have been intensively studied thus far. Among these H_2-related technologies, a H_2 gas sensor is a critical element for the safety of H_2 energy usage because leakage of even a small amount of H_2 gas may cause serious hazards, including fire and explosion [3,4]. In addition, H_2 gas-sensing technology can be utilized for other useful applications such as transformer failure detection [5–9] or exhaled-breath tests for the medical diagnosis of small intestinal bacterial overgrowth (SIBO) [10–12].

Metal-oxide semiconductors (MOSs) have drawn attention as H_2 gas-sensing materials for their high reaction speed and high sensitivity [13–19]. Among MOS-based sensing materials, SnO_2 has been extensively studied owing to its excellent chemical/physical properties such as high sensitivity and strong oxidizing power [20,21]. SnO_2 is an intrinsic n-type semiconductor with a bandgap energy of 3.6 eV at 300 K [21]. It has been proposed that the thickness of the electron depletion region in SnO_2 can be controlled by depositing noble metal catalysts such as Pd, Pt, and Au on the surface of SnO_2. Metal catalysts enable a large number of oxygen ion species to be adsorbed on the surface of the sensing materials, resulting in the formation of a thicker depletion layer through the extraction of electrons from SnO_2 [21,22]. In particular, Pd is known to be partially oxidized in air, forming a depletion layer in SnO_2, which is called electronic sensitization [23]. Furthermore, such catalysts stimulate the oxygen adsorption on the surface of SnO_2, the

* Corresponding author.
** Corresponding author at: Department of Materials Science and Engineering, Yonsei University, Seoul 03722, Republic of Korea.
E-mail addresses: h-slee@yonsei.ac.kr (H.-S. Lee), wooyoung@yonsei.ac.kr (W. Lee).

https://doi.org/10.1016/j.snb.2023.134350
Received 5 May 2023; Received in revised form 5 July 2023; Accepted 23 July 2023
Available online 24 July 2023

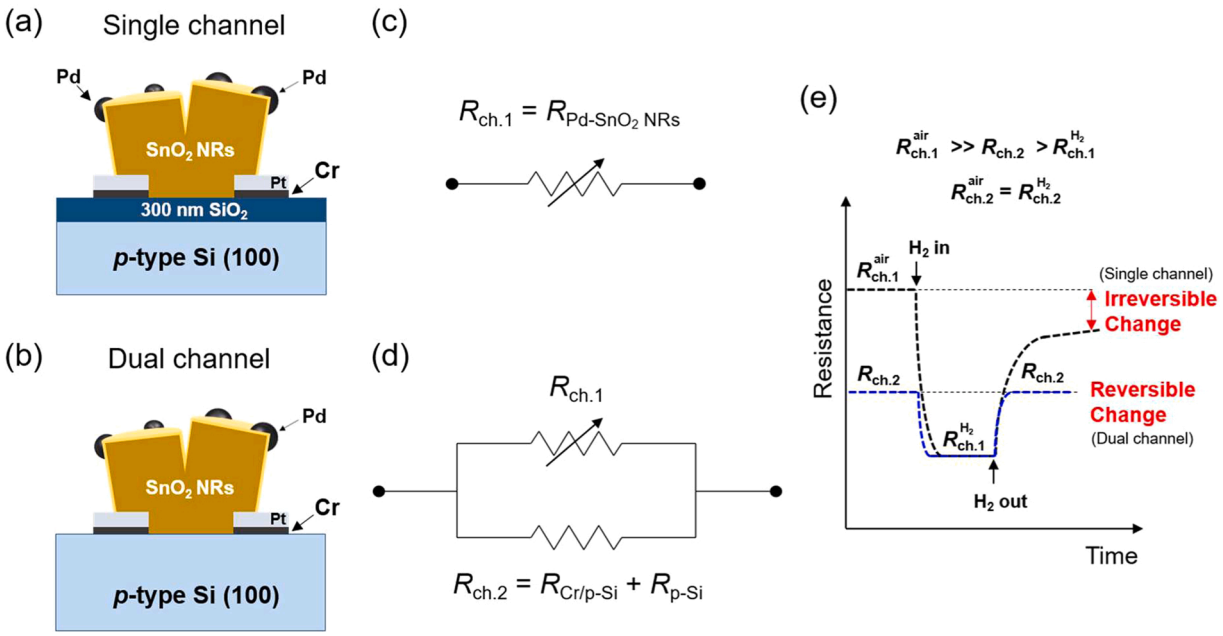

Fig. 1. Schematics of (a) single-channel and (b) dual-channel hydrogen (H_2) gas sensor systems, in which Pd-coated SnO_2 nanorods (NRs) were grown on (a) 300-nm SiO_2/p-type Si substrates and (b) p-type Si substrates, respectively. Interdigitated electrode (IDE) patterns of the Pt/Cr layer are integrated on both substrates. Simplified circuit diagrams for the (c) single- and (d) dual-channel H_2 gas sensor systems, respectively. Pd-coated SnO_2 NRs act as a single conduction channel on SiO_2/p-type Si (c), while the interface at Cr/p-type Si serves as a parallel conduction channel (d). The total resistance of the devices is expressed as $R_{total} = R_{ch.1}$ for the single channel and $1/R_{total} = 1/R_{ch.1} + 1/R_{ch.2}$ for the dual channel. (e) Graph of resistance change in the H_2 gas sensor during the H_2 in-and-out cycle. Irreversible resistance change is observed in the single-channel gas sensor system, whereas reversible resistance change is observed in the dual-channel gas sensor system.

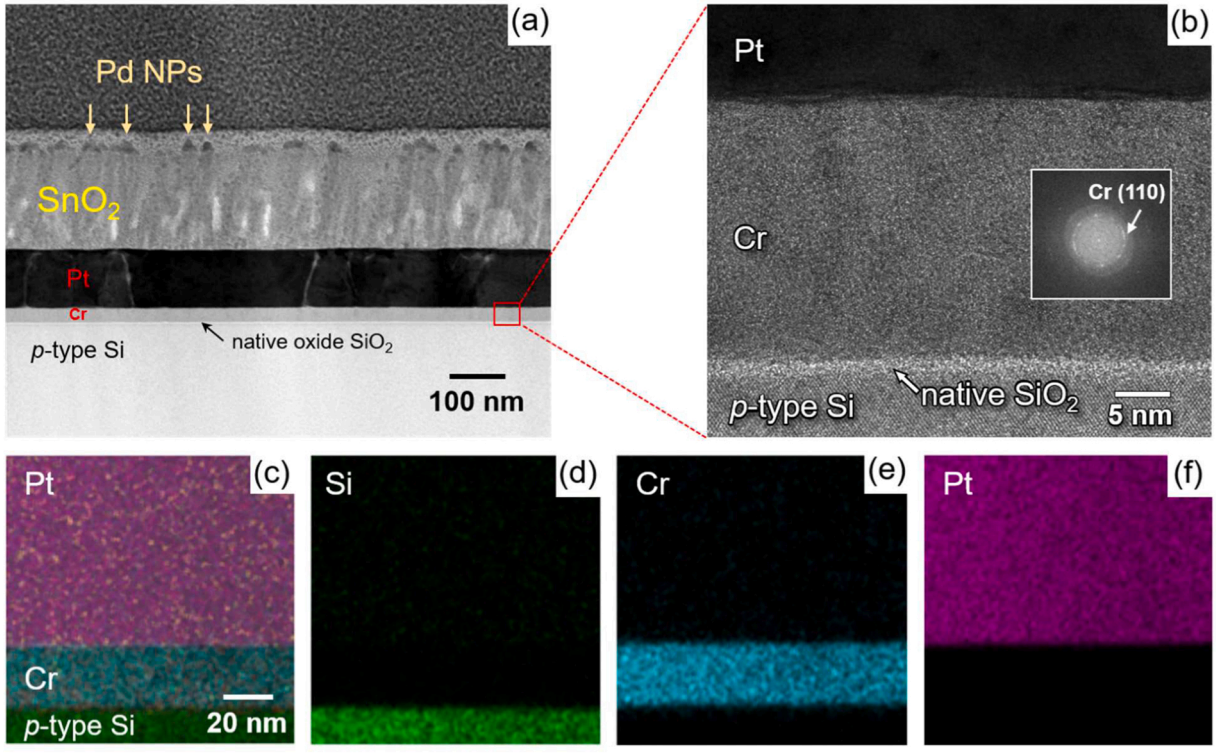

Fig. 2. (a) Low-magnification cross-sectional transmission electron microscopy (TEM) image of the dual-channel H_2 gas sensor. The region for SnO_2 NRs on the Pt/Cr IDE pattern is selected and observed. (b) High-resolution image taken from the selected area (red box in (a)). The metallic Cr phase is confirmed by the selected-area fast Fourier transform pattern (inset). (c–f) Energy-dispersive X-ray spectroscopy analysis of the cross-sectional TEM images with (c) Pt, Cr, and Si; (d) Si alone; (e) Cr alone; and (f) Pt alone.

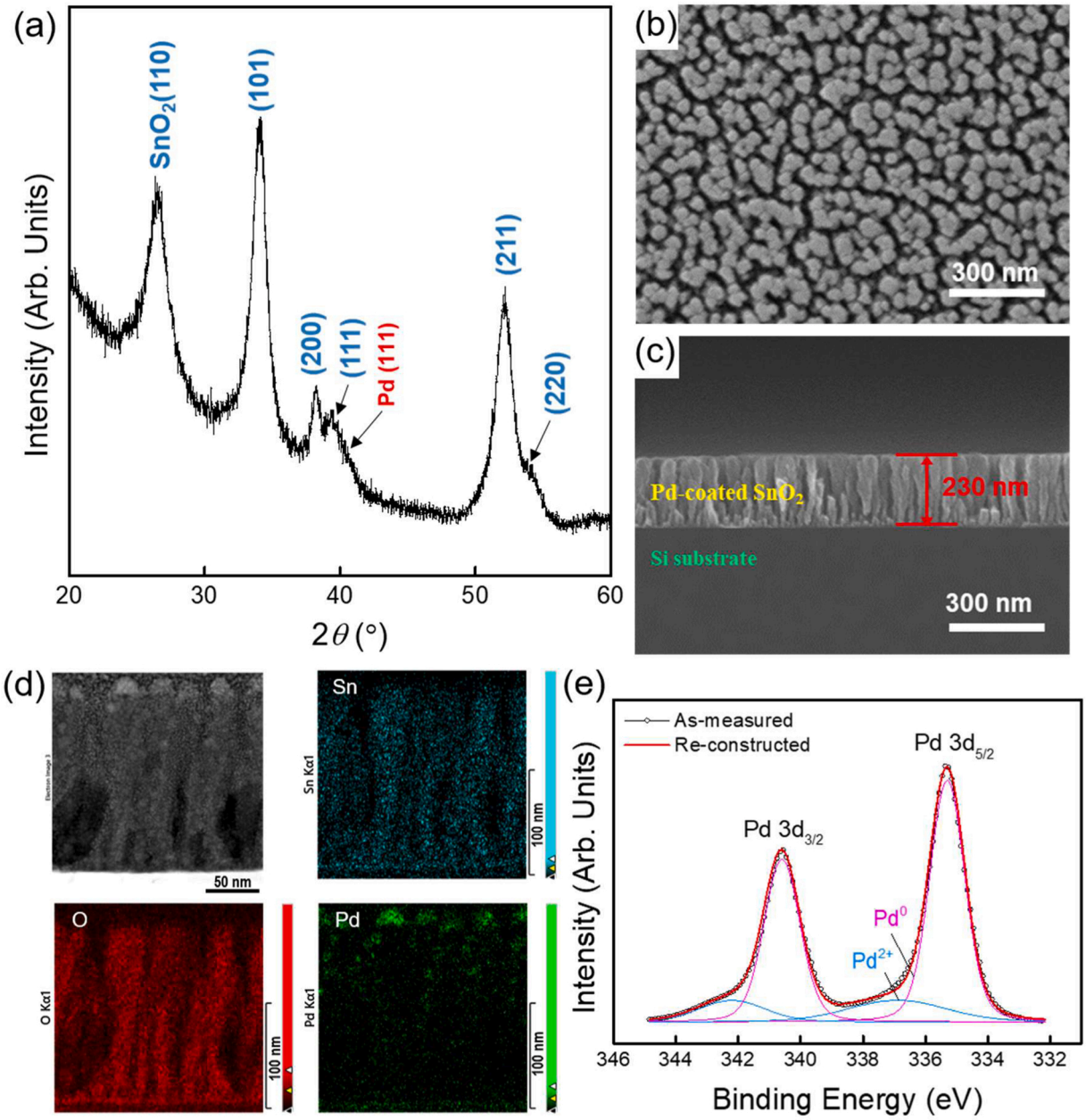

Fig. 3. (a) Grazing incidence X-ray diffraction pattern of Pd-coated SnO_2 NRs. The peak at $2\theta = \sim 40$ ° is related to the Pd (111) reflection. (b) Plane-view and (c) cross-sectional SEM images of Pd-coated SnO_2 NRs. (d) HR-TEM and EDS mapping images and (e) deconvoluted XPS Pd 3d spectrum of Pd-coated SnO_2 NRs.

so-called spillover effect [9], causing an increment in the resistance of SnO_2 [9,23]. If H_2 gas is introduced, the adsorbed oxygen reacts with H_2 and is removed from the surface of the sensor. Through this reaction, electrons bound to the surface oxygen return to SnO_2; therefore, the resistance of SnO_2 is reduced. To achieve high sensitivity toward H_2 gas, a large surface area is important for more efficient surface reaction of the sensor. Accordingly, nanostructures such as nanoparticles (NPs) [24], nanorods (NRs) [9,25,26] and nanowires [8] are frequently used with the incorporation of metal catalysts [8,9,23,27–31] on top of them. Regarding the commonly used metal catalysts, there have been numerous studies on H_2 gas sensors based on Pd-decorated MOS nanostructures because Pd exhibits high reactivity with H_2 gas [8,9,23,29,32,33].

However, a drawback of MOS-based H_2 gas sensors is the high sensing temperature (>200 °C) required for their optimal functionality [15,17,20,21,23–25]. At a lower temperature range (below 100 °C), which is important for wide applications [3,4,34–38], the activation energy is insufficient for a fast and reversible oxygen-adsorbed state on the surface of the sensor material during the H_2 in-and-out cycle, resulting in slow and irreversible resistance changes in the sensors. Notably, not only response speed but also reversible resistance changes with respect to H_2 concentration and temperature is important for practical applications because a high-resistance state without H_2 gas is required as a baseline resistance for signal calculations in the device. To address this issue and provide a reliable baseline resistance for the sensor, the idea of adding an extra electron-conduction channel, which can serve as the main conduction channel without H_2 gas, has been proposed [39–44]. For example, graphene has been investigated for preparing the extra electron-conduction channel; however, there is a limitation for applications because of their low stability and productivity [39–44].

In this work, we demonstrate highly stable and reversible H_2 sensors based on Pd-coated SnO_2 NRs, utilizing a Cr/native oxide/p-type Si Schottky barrier interface as a parallel electron-conduction channel. An

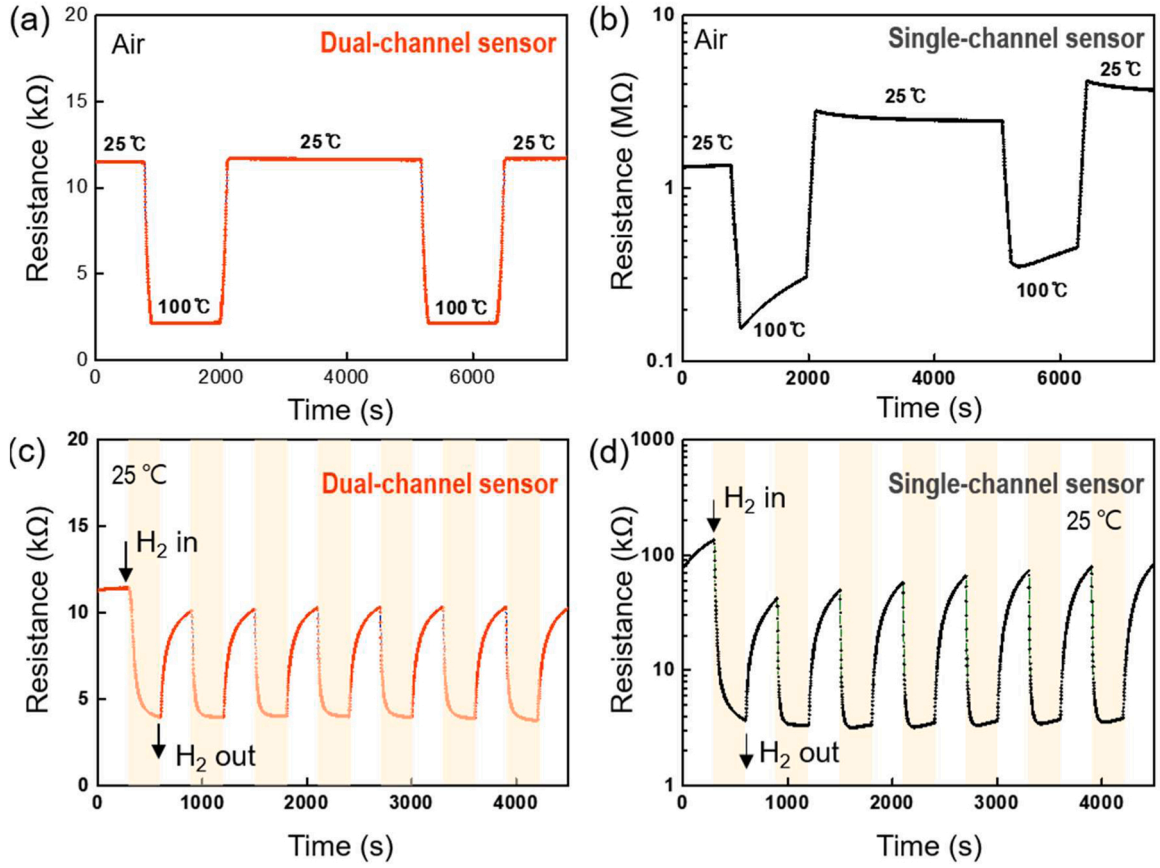

Fig. 4. Resistance changes in the (a) dual-channel and (b) single-channel H_2 gas sensor with respect to the temperature change in dry air. Resistance changes in the (c) dual-channel and (d) single-channel H_2 gas sensor during the H_2 gas in-and-out cycle. Air-balanced H_2 gas (500 ppm) was used for the measurement at 25 °C.

optimal baseline resistance of the second conduction channel is successfully achieved with the Schottky barrier height, as revealed by the work function and chemical stability between Cr and p-type Si. The dual-channel sensor exhibited reversible resistance change during H_2 gas in-and-out cycles at temperatures between 25 °C and 100 °C. The optimal working temperature of the dual-channel sensor developed in this research was 80 °C, which enabled practical H_2 sensor applications. Moreover, the dual-channel sensor exhibited significantly high sensitivity and reliable sensing performance, which could be employed in various H_2 sensor applications.

2. Materials and methods

2.1. Sensor fabrication

Bare p-type Si < 100 > and thermally grown SiO_2 (300 nm)/Si substrates (525 μm) were used to fabricate single- and dual-channel sensors, respectively. The resistivity of p-type Si < 100 > wafers was in the range of 1–10 Ω·cm. Pt/Cr interdigitated electrodes (IDEs) were fabricated on substrates using photolithography. The width and spacing of digits in IDEs were 50 μm and 10 μm, respectively. A Pt (100 nm)/Cr (20 nm) IDE was deposited by DC magnetron sputtering, where the power, working pressure, and Ar flow were set to 32 W, 2 mTorr, and 34 sccm, respectively. Sputter cleaning of the substrate was not performed prior to the electrode deposition to retain the native oxide on Si substrates. The 20-nm Cr layer was selected as the adhesion and interface layer with SiO_2/Si substrates. After the formation of IDEs on the substrates, SnO_2 NRs were deposited using the glancing angle deposition method. The samples were tilted at 80° and rotated at a speed of 12 rpm in the vacuum chamber of an e-beam evaporator (KVE-E2000, Korea Vacuum Tech). The SnO_2 NRs were deposited under an initial base pressure of ~2.0×10^{-6} Torr and deposition rate of 1.0 Å/s by using commercial SnO_2 granules (99.99%, Kojundo Chemical Laboratory) inside a 7-cc crucible for 1700 s. After deposition, the samples were annealed at 550 °C for 2 h in atmospheric air using a tube furnace (Korea Furnace Development Co., Ltd). Pd catalyst with an optimal thickness of 5 nm was deposited on vertical SnO_2 NRs using a DC magnetron sputtering system (SNTEK Co., Ltd). A working gas pressure of 2 mTorr with 34-sccm Ar and a deposition rate of 3.6 Å/s at 20 W were used for Pd deposition. The schematic of the overall fabrication process for SnO_2 nanorods with Pd nanoparticles is presented in Fig. S1.

2.2. Characterization

The crystalline structure of Pd-coated SnO_2 NRs was analyzed using an X-ray diffractometer (SmartLab, Rigaku) with Cu $K\alpha_1$ radiation (λ = 1.5409 Å). The surface morphology of the samples was investigated using field emission scanning electron microscopy (FE-SEM, JEOL-7800 F, JEOL Ltd.). The overall laminated structure of the sensor (sensing material/electrode/substrate) was investigated using high-resolution transmission electron microscopy (HR-TEM, JEM-ARM 200 F NEOARM, JEOL Ltd.) equipped with energy-dispersive X-ray spectroscopy (EDS). The chemical state of the Pd catalyst was analyzed by X-ray photoelectron spectroscopy (XPS, K-alpha Thermo U. K.) using Al Kα radiation.

2.3. Gas-sensing measurement

The fabricated sensors were loaded in a commercial chamber comprising a two-probe system and a Peltier stage in a chamber (volume = 100 cc, Micro Probe System, Nextron). The sensor resistance was measured by applying a constant current (1 μA) for an interval of 1 s

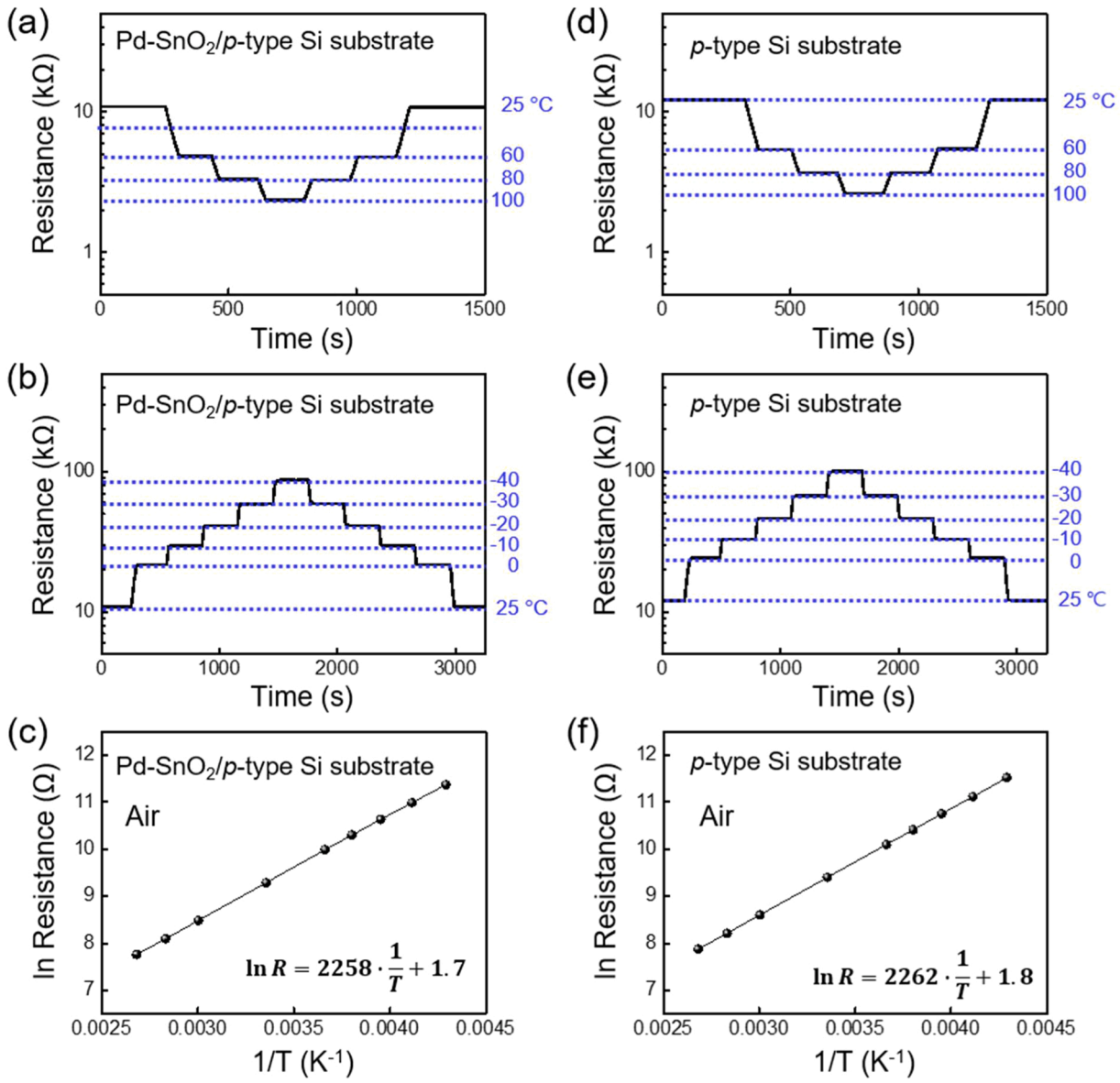

Fig. 5. Resistance changes in Pd-coated SnO_2 NRs on the IDE-patterned *p*-type Si substrate with respect to temperature change in the temperature range of (a) 25–100 °C, (b) − 40–25 °C. (c) Log resistance vs. $1/T$ plot for Pd-coated SnO_2 NRs on the IDE-patterned *p*-type Si substrate. Resistance changes in the IDE-patterned *p*-type Si substrate (without SnO_2) with respect to temperature change in the range of (d) 25–100 °C, (e) − 40–25 °C. (f) Log resistance vs. $1/T$ plot for the IDE-patterned *p*-type Si substrate.

with a measurement unit (Keithley 236 SMU, Keithley Instruments Inc.). The operating temperature of the sensors on the Peltier stage was controlled by a computer program with a constant ramping rate (~40 °C/min). The H_2 gas flow rate with various concentrations diluted in dry air was fixed at 1000 sccm by a mass flow controller.

To analyze sensing properties, the response is defined as $(R_a - R_g)/R_g$, where R_a and R_g are the resistances before and after H_2 exposure, respectively. Response and recovery times are defined as the time required to reach 90% of total decreasing resistance changes upon exposure to H_2 gas of various concentrations and time to recover 90% of total changes after removing H_2 in dry air, respectively.

3. Results and discussion

Fig. 1(a) and (b) show the schematics of the single- and dual-channel H_2 gas sensor systems. For the conventional single-channel sensor, the sensing material of Pd-coated SnO_2 NRs was deposited on the IDE-patterned substrate of electrically insulating SiO_2 (300 nm)/Si. In such a case, Pd-coated SnO_2 NRs represent the only electron-conduction channel, and their resistance ($R_{ch.1}$) changes are directly linked to sensing performance (Fig. 1(c)). In general, MOS-based gas sensors such as SnO_2 have a high optimal working temperature above 200 °C. Therefore, at a low operating temperature (below 100 °C), which is the preferred sensing temperature for applications, H_2 atoms adsorbed on Pd are not completely desorbed after the sensing reaction. This causes irreversible baseline-resistance changes during the H_2 in-and-out cycle (Fig. 1(e)). The detailed mechanism of oxygen adsorption/desorption, H_2 in-and-out cycle, and the resultant resistance changes will be discussed later in this paper.

Meanwhile, if there is a second electron-conduction path with an appropriate resistance, its resistance can be used as a baseline resistance for sensor signal calculation because the irreversible high-resistance baseline observed in the single-channel sensor can be avoided during the H_2 in-and-out cycle. To realize stable base resistance of the sensor device (Fig. 1(b)), we selected a Cr electrode and electrically conductive bare p-type Si substrate instead of the thermally oxidized SiO_2

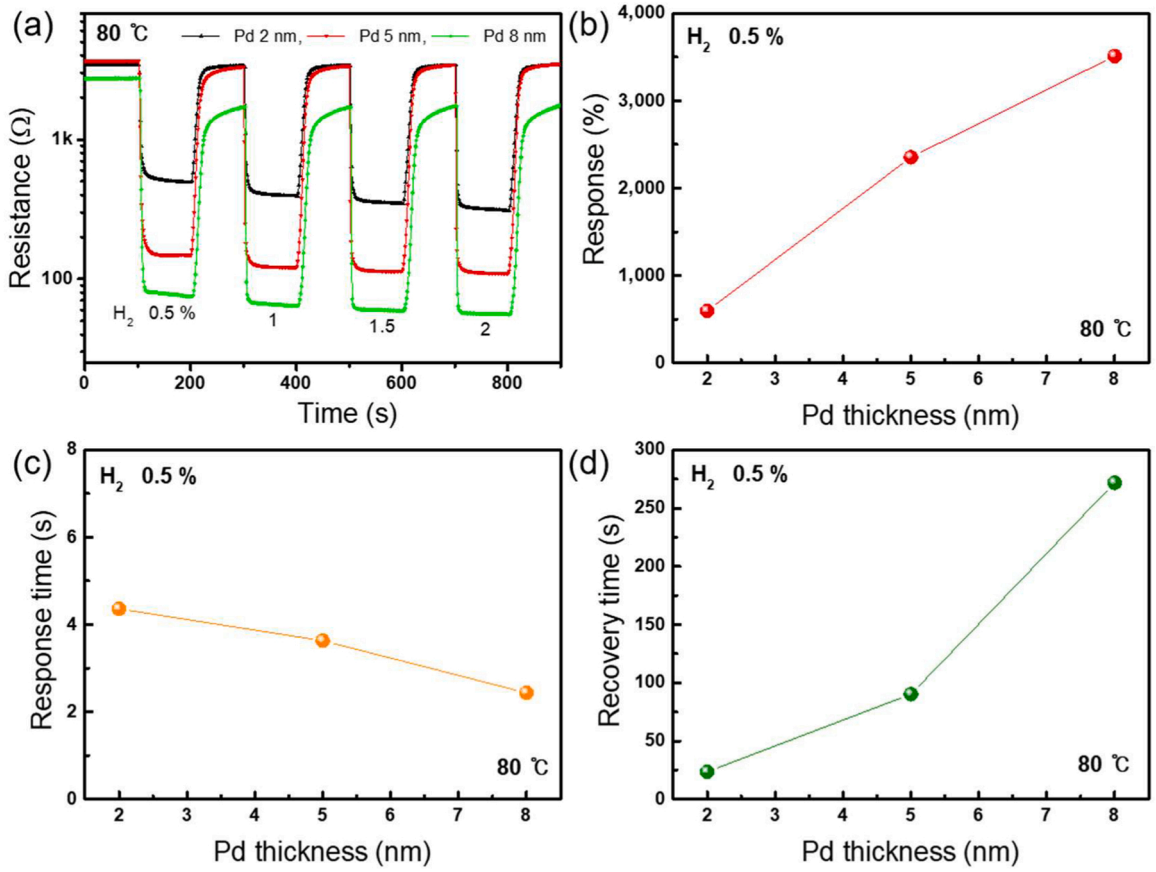

Fig. 6. (a) Variation in the resistance of the dual-channel Pd-SnO_2 NRs sensors prepared with different Pd thickness (2, 5, and 8 nm) for H_2 concentration range of 0.5%– 2%, (b) response, (c) response time, and (d) recovery time of the sensors as a function of Pd thickness.

(300 nm)/Si substrate, which is typically used for the fabrication of MOSs gas sensors. In this case, the electron-conduction path through the interface of Cr/p-type Si ($R_{Cr/p\text{-}Si}$) and p-type Si ($R_{p\text{-}Si}$) becomes the second channel ($R_{ch.2}$) in addition to the first conduction channel ($R_{ch.1}$), which comprises Pd-coated SnO_2 NRs (Fig. 1(d)). Because of the difference in the work function of Cr and p-type Si (Fig. S2), the interface can form a Schottky barrier, which may provide the resistance level that can be used as the baseline resistance of the sensor. Therefore, this resistance level during the recovery from H_2 exposure is the same as the initial baseline resistance value prior to exposure to H_2 gas, resulting in reversible resistance change during the H_2 in-and-out cycle (Fig. 1(e)). Because this approach does not require any extra process or material such as graphene [40–43] to create the second path for electron conduction, the fabrication process is more manufacturable and cost-effective in comparison to the multi-layered sample structure.

Fig. 2(a) shows the cross-sectional transmission electron microscopy (TEM) image of Pd nanoparticles (Pd NPs)/SnO_2 NRs/Pt/Cr/native oxide/p-type silicon, clearly revealing the well-defined interfaces of all layers of SnO_2, Pt, Cr, native oxide, and p-type Si substrate. The enlarged image near the interface between Cr and the *p*-type Si substrate is shown in Fig. 2(b). From the selected-area fast Fourier transform pattern (Fig. 2 (b) inset), the existence of a metallic Cr layer was confirmed. The thicknesses of Cr and the native oxide (SiO_2) were found to be ~20 and ~1.7 nm, respectively. From the EDS mapping results (Fig. 2(c)–(f)), we found that there was no significant intermixing among Pt, Cr, and p-type Si.

The native oxide between Cr and the p-type Si interface can modify the electronic structure of Cr and p-Si; therefore, the Schottky barrier height is also modified [44–46]. The modified barrier height will determine the actual resistance of the second-channel electron conduction ($R_{ch.2}$) of the device. Through the incorporation of the native oxide with an appropriate thickness, the resistance of the second current channel can be tuned to achieve optimal baseline resistance in the device. However, the thickness of the native oxide is self-limiting in nature depending on the environmental condition and is not easy to tune as needed. Alternatively, the native oxide can be replaced with other materials that can be processed with more precise control of thickness and thereby barrier height and resistance [41,42]. Further investigation is required to characterize the barrier height of the Cr/native oxide/p-Si interface and determine its effect on the electron transport behavior and the interface resistance in this system.

The information on the crystalline structure and morphologies of Pd-coated SnO_2 NRs is presented in Fig. 3. The XRD patterns indicate that the as-prepared Pd-coated SnO_2 NRs were well crystallized without secondary or impurity phases (Fig. 3(a)). The plane-view (Fig. 3(b)) and cross-sectional (Fig. 3(c)) SEM images show that the SnO_2 NRs were grown to average dimensions of ~230 nm (in length) and 20–30 nm (in diameter). The elemental analysis using HR-TEM revealed that clusters of Pd catalysts were capped on the top surface of NRs and also distributed on the side of the NRs (Fig. 3(d)). The chemical state of Pd was analyzed using XPS measurements. The XPS Pd 3d spectrum of Pd-SnO_2 NRs was deconvoluted to identigy the pure metallic Pd state (P^0) and oxidized PdO state (Pd^{2+}) (Fig. 3(e)). The binding energies of Pd $3d_{5/2}$ for native P^0 and oxidized Pd^{2+} states are known to be in the range of 335.1–335.4 eV and 336.8–337.2 eV, respectively [47]. As shown in Fig. 3(e), the Pd $3d_{5/2}$ peaks were deconvoluted into a dominant P^0 peak at ~335.3 eV and a less prominent Pd^{2+} peak at ~336.8 eV. These results suggest that the Pd coated onto the SnO_2 NRs primarily consists of a metallic phase with some degree of oxidation.

To verify the dual-channel sensing behavior, we compared the

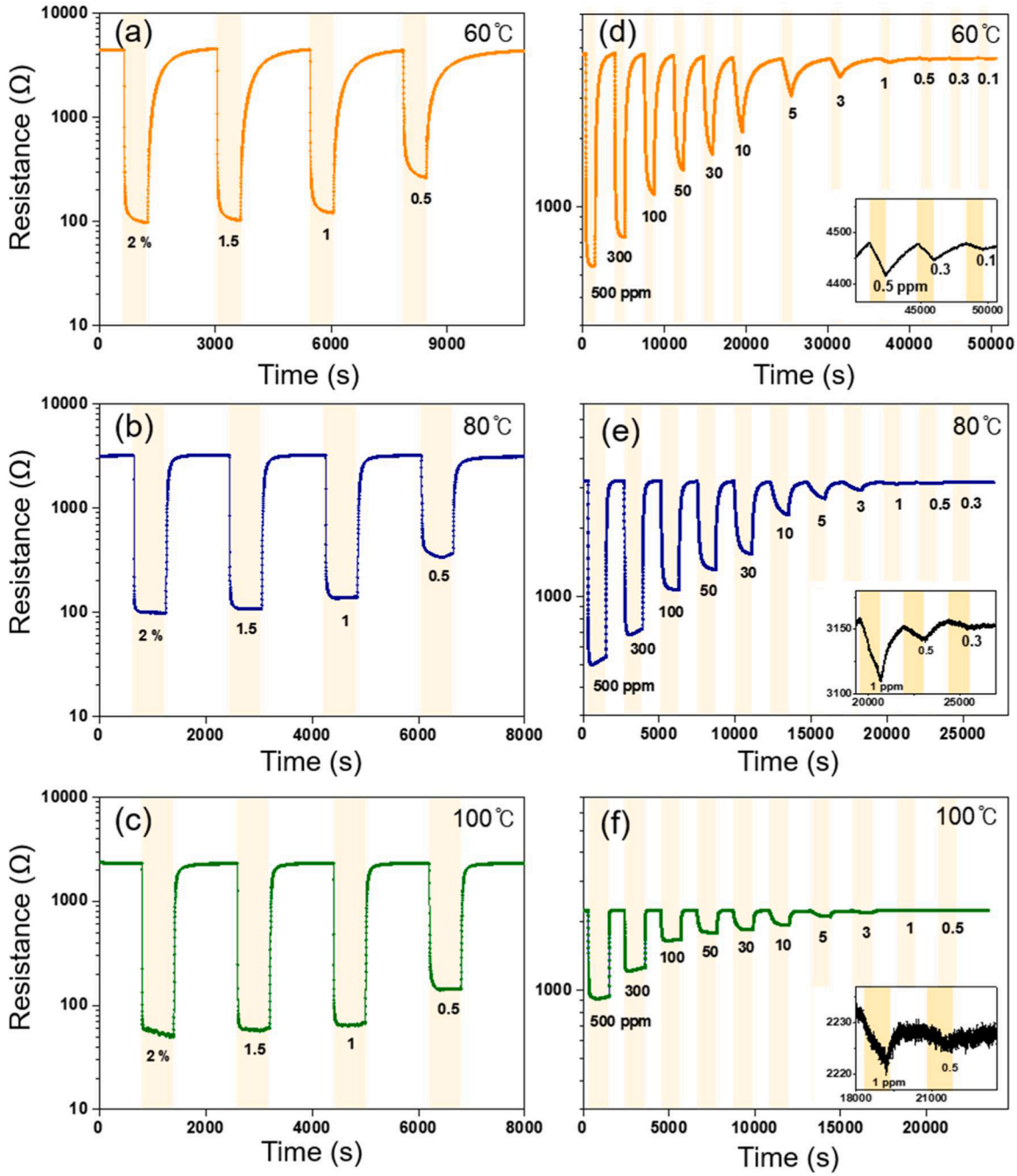

Fig. 7. Variation in the resistance of the dual-channel H_2 gas sensor at H_2 concentration ranges of (a)–(c) 0.5%– 2% and (d)–(f) 0.1–500 ppm and different operating temperatures: 60 °C, 80 °C, and 100 °C. A reaction time of 1200 s was used for each H_2 concentration.

resistance change with respect to the temperature and H_2 in-and-out cycle for both single- and dual-channel sensors. Fig. 4(a) shows the resistance change of the dual-channel sensor when the temperature is changed from 25 °C to 100 °C repeatedly in dry air. In this case, the electron conduction is carried out through the second channel because the sensor material is not exposed to H_2 and maintains higher resistance ($R^{air}_{ch.1}$) than the second path resistance ($R_{ch.2}$) at 25 °C as well as 100 °C. The resistance of the device at 25 °C and 100 °C is mainly due to the temperature dependence of the Schottky barrier height at the Cr/native oxide/p-Si interface. Therefore, the temperature dependence of gas adsorption and desorption dynamics did not contribute to the device resistance, and the resistance changes were reversible and stable with the temperature change cycle in the dual-channel sensor.

In the case shown in Fig. 4(b), the resistance is mainly governed by the chemisorption reaction of oxygen ion species on the surface of the sensor material of Pd-SnO_2 NRs at 25 °C and 100 °C. The behavior of the resistance in the single-channel sensor was irreversible and unstable during heating and cooling cycles. The change in resistance curves with different temperatures reflects the bulk resistance corresponding to the intrinsic electronic properties of the sensing material and the surface resistance affected by the adsorbed oxygen ion species [38]. As shown in Fig. 4(b), the resistance at 100 °C is lower than that at 25 °C, which reflects the semiconducting bulk properties of the sensor material. In addition, at 100 °C, the resistance value and the slight increase in it with time are almost similar for repeated heating and cooling processes. This is because the species and quantities of adsorbed oxygen are specified at the temperature of 100 °C [38]. However, higher resistance was

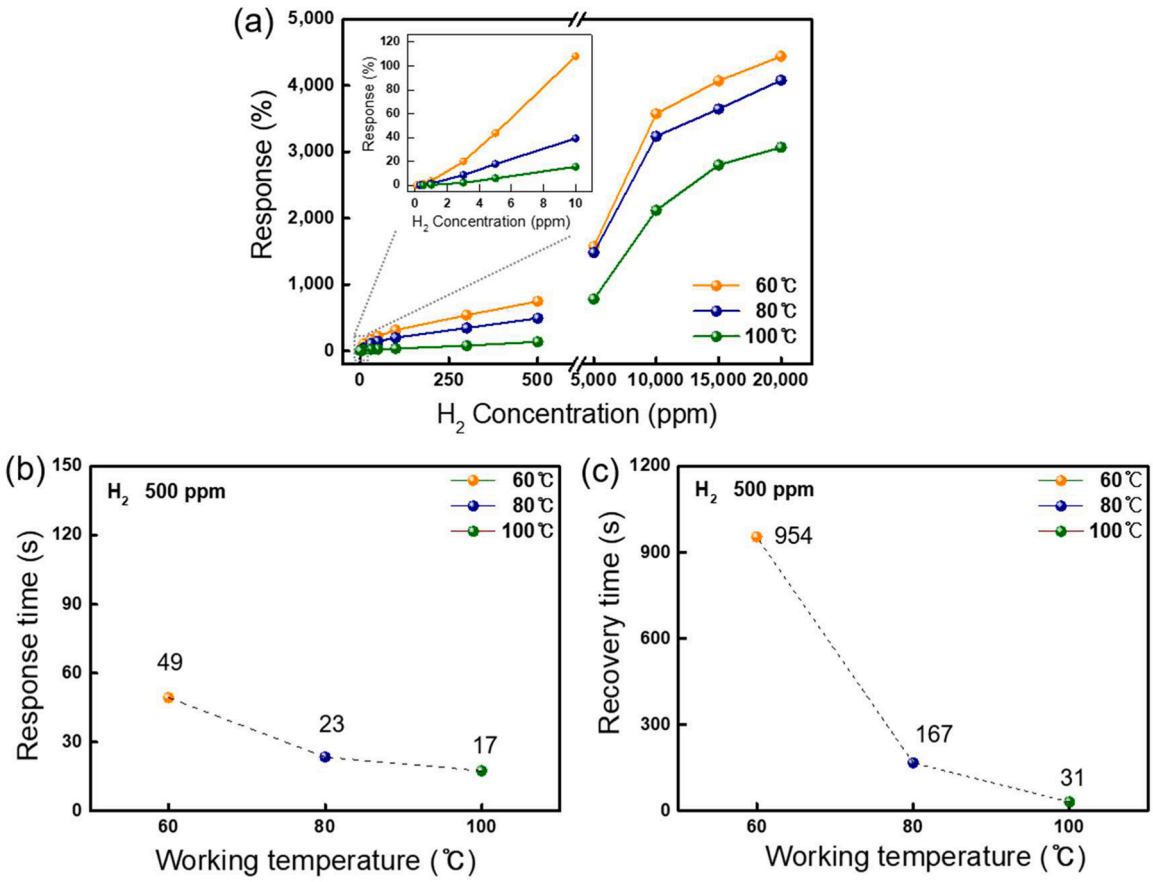

Fig. 8. Temperature dependence of sensing performance of the dual-channel hydrogen gas sensor: (a) Maximum response under 0.1–500 ppm and 0.5%– 2% H_2 (response = $\Delta R/R_g \times 100$ (%)); (b) response and (c) recovery time under exposure to 500-ppm H_2. The response and recovery time were estimated using the following definition: the time required to reach 90% of the total change in response and recovery.

observed after cooling from 100 °C to 25 °C. This can be attributed to the abundance of chemisorbed oxygen and nonequilibrium state generated by the cooling process [38]. This irreversible and unstable baseline resistance depending on the temperature is the main drawback of the single-channel sensor for practical applications.

Moreover, the behavior of resistance change at 25 °C was reversible during the H_2 in-and-out cycle in the dual-channel sensor (Fig. 4(c)), which was in contrast to the behavior in the single-channel sensor (Fig. 4 (d)). The single-channel sensors did not exhibit complete recovery under identical measurement conditions. When H_2 gas was introduced into the sensor, it reacted with the chemisorbed oxygen to produce H_2O. Electrons generated in this chemical reaction were released back into the conduction band of the sensing material, thereby reducing the resistance of the sensor. Further, when H_2 gas was removed from the sensor and air was injected, the resistance of the Pd-SnO_2 sensor increased again, and the conduction path switched from the first to the second path when the sensor resistance reached that of the second conduction channel. Fig. 4 (c) shows the repeating resistance pattern with a baseline resistance of 10 kΩ according to the H_2 in-and-out cycle at 25 °C. The resistance of the sensor reliably and repeatedly changed between 10.3 and 3.6 kΩ according to the H_2 gas in-and-out cycles in the dual-channel sensor.

If the baseline resistance of the dual-channel sensor is determined by the interface of Cr/native oxide/p-type Si and p-type Si substrate as shown in Fig. 4(c), this resistance value is also expected to be comparable with that of the IDE-patterned p-type Si substrate without SnO_2 NRs. To verify this hypothesis, we compared the resistance changes in IDE-patterned p-type Si substrates with and without Pd-coated SnO_2 NRs. Fig. 5(a) and (b) clearly reveal the stable and reversible behavior of the dual-channel sensor under the wide temperature range of − 40–100 °C in air. This resistance value at each temperature is almost identical to that in IDE-patterned p-type Si without SnO_2 NRs, as shown in Figs. 5(d) and 5(e). From the identical behavior in log resistance vs. $1/T$ for IDE-patterned p-type Si with and without SnO_2 NRs (Figs. 5(c) and 5(f), respectively), we confirmed that the baseline resistance in the dual-channel sensor is governed by the interface at Cr/native oxide/p-type Si. Furthermore, this result suggests that the interface resistance can be explained by the Schottky barrier height model [48,49], thereby validating our hypothesis regarding the band diagram for Cr/native oxide/p-type Si (Fig. S2). This unambiguously reveals that the baseline resistance in the dual-channel sensor originates from the interfacial resistance. Meanwhile, the baseline resistance (R_a), derived from the interfacial resistance, exhibits a constant value with temperature dependence and it decreases with increasing temperature, as shown in Fig. 5(d). The fixed value of the baselines resistance in the dual-channel sensor can provide information about the operating temperature. This advantageous characteristic allows the parallel second conduction channel to serve the same purpose as a temperature sensor. In terms of commercialization, when using a dual-channel sensor, it may not be necessary to incorporate a separate temperature sensor.

Before evaluating the sensing ability of the dual-channel sensor, we optimized the thickness of the Pd catalyst using various dual-channel Pd-SnO_2 NRs sensors prepared with different Pd thicknesses (2, 5, and 8 nm). Fig. 6(a) shows the resistance variations over time at the operating temperature of 80 °C for various hydrogen concentrations (0.5%, 1%, 1.5%, and 2%). The response was calculated using a definition of $\Delta R/R_g \times 100$ (%), where $\Delta R = R_a - R_g$. Here, R_a and R_g are the resistances of the sensor in air and hydrogen, respectively. The response time and recovery time were estimated as the time required to reach

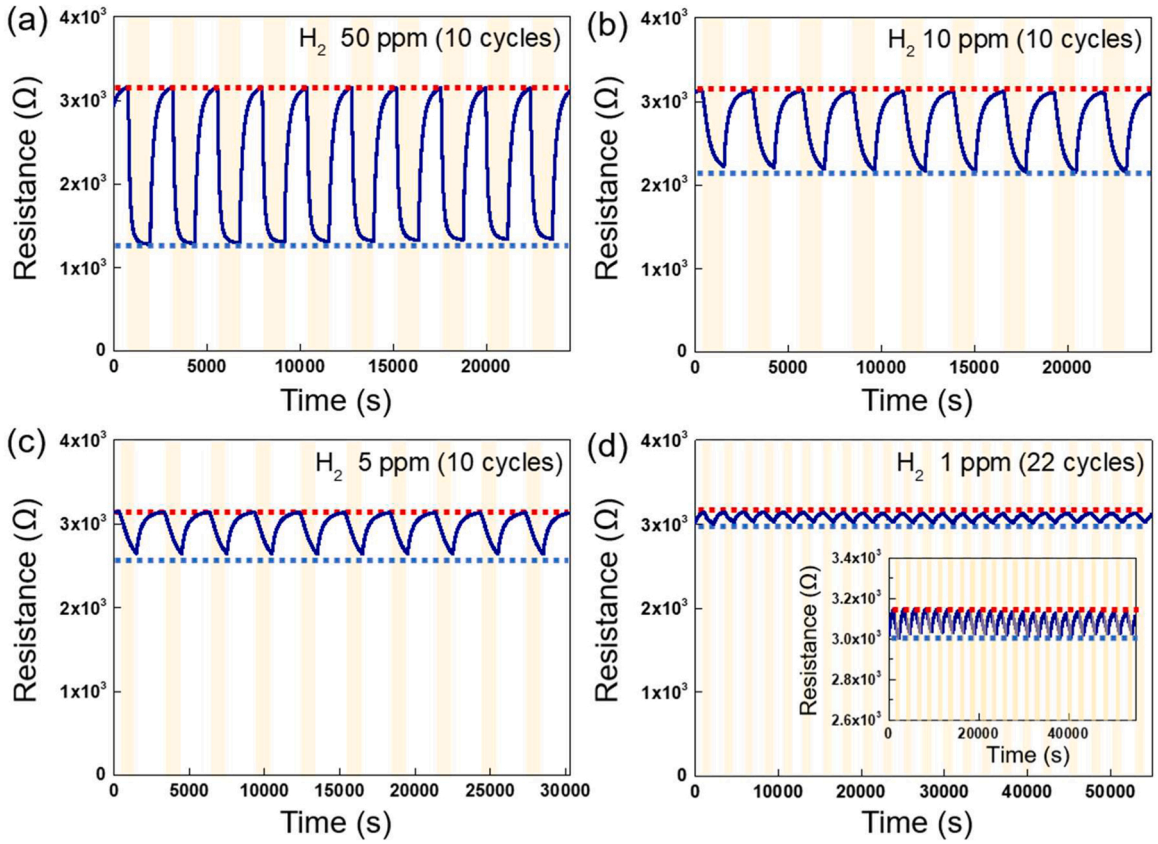

Fig. 9. Sensing reproducibility tests of the dual-channel H_2 gas sensor for H_2 gas concentrations of (a) 50, (b) 10, (c) 5, and (d) 1 ppm at the operating temperature of 80 °C.

90% of the saturated response and recovered base-resistance, respectively. With increasing Pd thickness increases, the sensors exhibited higher sensing response (Fig. 6(b)) and faster response time (Fig. 6(c)), attributed to the enhanced reactivity resulting from a larger amount of catalyst. However, the recovery time is significantly increased (Fig. 6 (d)). Thus, the optimal thickness of Pd was 5 nm, which was selected based on criteria such as high response and short response/recovery time.

To evaluate the sensing performance of the dual-channel Pd(5 nm)-SnO_2 NRs sensor for applications at relatively lower temperatures (< 100 °C) than those for the conventional sensor operation (>200 °C), its resistance was evaluated at 60–100 °C under high and low concentrations of hydrogen in the ranges of 0.5%– 2% (Fig. 7(a)–(c)) and 0.1–500 ppm (Fig. 7(d)–(f)), respectively. As shown in Fig. 7, the dual-channel sensor exhibited an excellent response/recovery characteristic with a stable baseline resistance in the different ranges of H_2 concentration at each temperature. Notably, these baseline resistances are the same as the interfacial resistance, which is shown in Fig. 5 at temperatures of 60 °C (Fig. 7(a) and (d)), 80 °C (Fig. 7(b) and (e)), and 100 °C (Fig. 7(c) and (f)). The sensing response of the dual-channel sensor increased with an increase in H_2 concentration, and the sensitivity (slope) was different at each H_2 concentration range (Fig. 8). As the temperature increased, the response of the dual-channel sensor decreased (Fig. 8(a)) because the interfacial resistance decreased at higher temperatures (Fig. 5(d)). However, the response/recovery time can be faster at higher temperatures (Fig. 8(b)) owing to a higher reaction rate on Pd-SnO_2 NRs [20–23,35,37,50,51]. In particular, the recovery time at 100 °C can be reduced to ~31 s, which is very fast compared to typical MOS-based single-channel sensors. Consequently, the optimal operating temperature of the dual-channel sensor was found to be 80 °C, which satisfied requirements such as high response and high response/recovery speed with a stable and reversible baseline resistance. A low detection limit of the dual-channel sensor was observed, reaching 0.5 ppm at the optimal working temperature of 80 °C (Fig. 7(e)). It is noteworthy that the dual-channel sensor is capable of detecting H_2 concentrations as low as 0.5 ppm, even at this low operating temperature. Moreover, the measurement results using 1% H_2 gas (Fig. S3) showed fast sensing response within 2 s. These results indicate that the dual-channel Pd-coated SnO_2 NRs sensor is suitable for applications such as hydrogen leak detectors that require high speed and precision. Because the sensor can detect low H_2 concentrations, if the baseline resistance or barrier height is further optimized, the response and response time could be further improved, and the sensor could be used in applications such as a hydrogen breath analyzer.

We compared the sensing properties of the dual-channel sensor with those of the single-channel sensor at 80 °C (Fig. S4). The sensing resistance curves of the single-channel sensor were obtained under the same measurement conditions, including exposure time to air–H_2–air, H_2 concentration, and operating temperature. As shown in Fig. S4(a), the resistance of the single-channel sensor does not exhibit reversible recovery to its initial state. This lack of recovery implies that the baseline resistance (R_a) after the sensing measurement is not consistently maintained, leading to inaccurate response calculations. When the response of the single-channel sensor was calculated using different R_a values for each H_2 concentration, the single-channel sensor exhibited a lower response and a different curvature compared to the dual-channel sensor. Both sensors exhibited a response time of less than 2 s (Fig. S4(d) and (e)). However, as shown in Fig. S4(e), the single-channel sensor required a significantly longer time to observe the fully recovered initial state after detection of 2% H_2.

We performed reliability and long-term stability tests of the dual-channel sensor at 80 °C. The results of the repeatability test (Fig. 9) showed that the resistance changes for low H_2 concentrations of 50, 10, 5, and 1 ppm were highly reproducible during 10 or 22 cycles of sensing

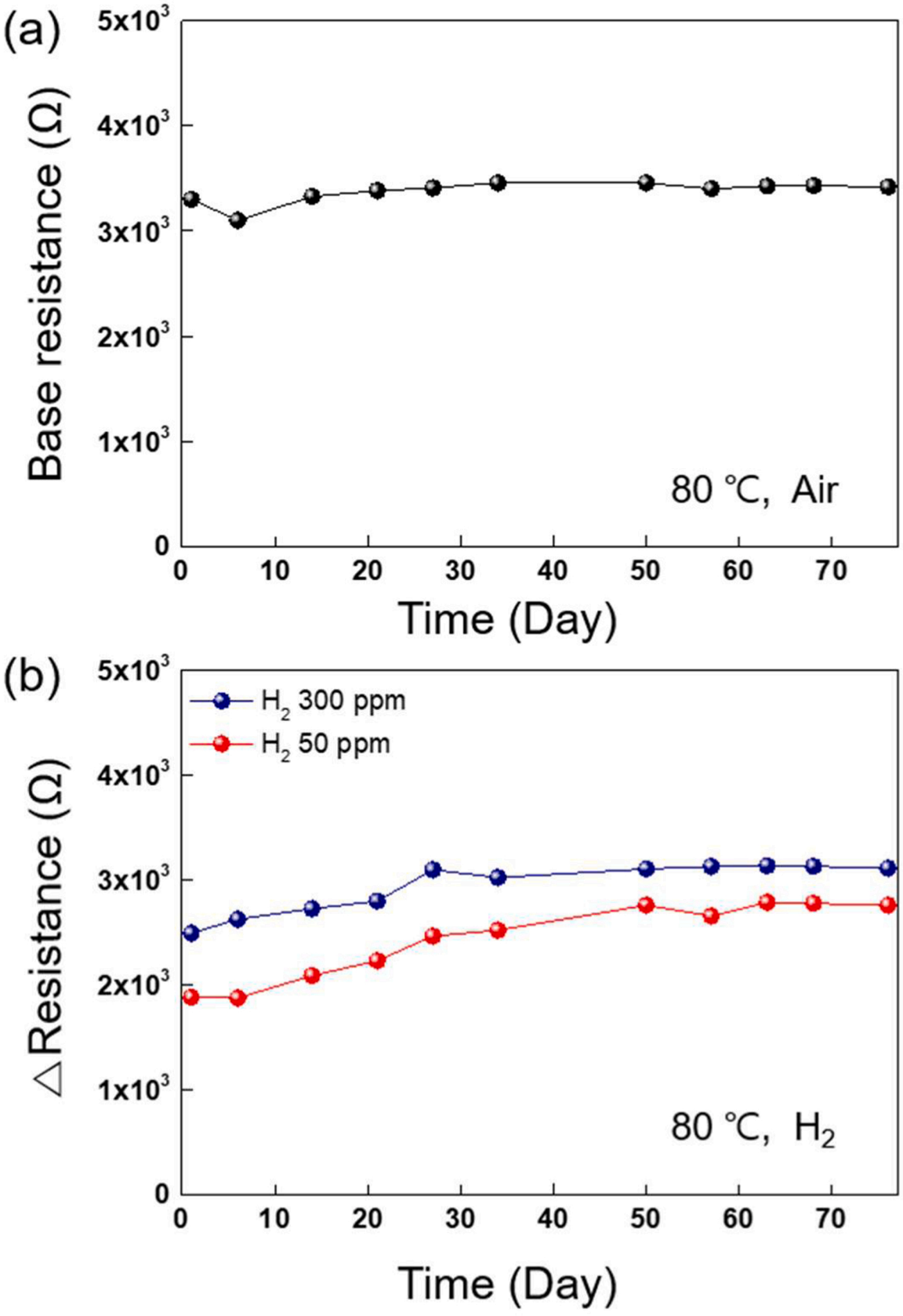

Fig. 10. Long-term stability test of the dual-channel H_2 gas sensor at 80 ℃ for 76 days: (a) Base resistance of the sensor in air and (b) resistance change of the sensor upon exposure from air to H_2 at 50 and 300 ppm.

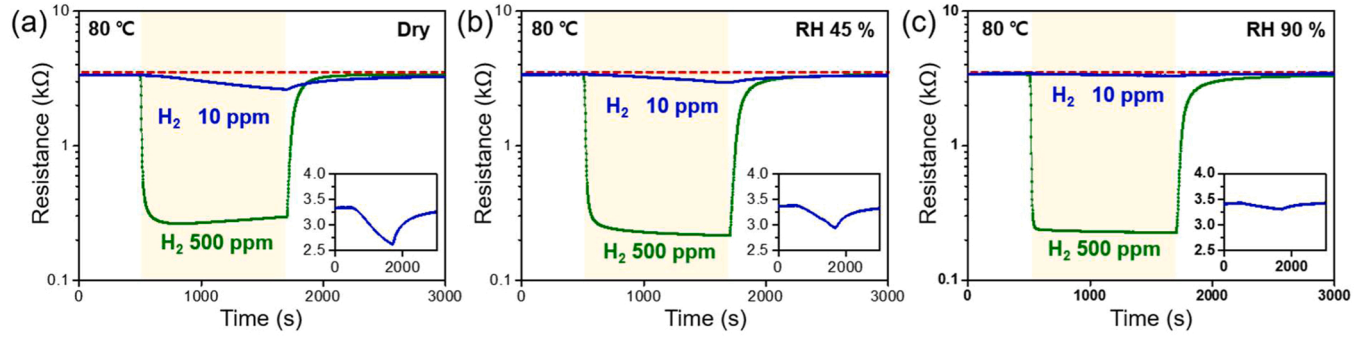

Fig. 11. Humidity effect of the dual-channel H_2 gas sensor at 80 ℃: resistance variation curves in time for 500 and 10 ppm H_2 under (e) dry, (b) RH 45%, and (c) RH 90% humid atmosphere. The humidity conditions were prepared at 22 ℃. During the sensing test, the sensor operating temperature was adjusted to 80 ℃ using a Peltier plate, and the H_2 gas containing RH 45% and RH 90% prepared at 22 ℃ was injected into the sensor chamber. Therefore, only the sensor was heated to 80 ℃ and the test gas was 22 ℃.

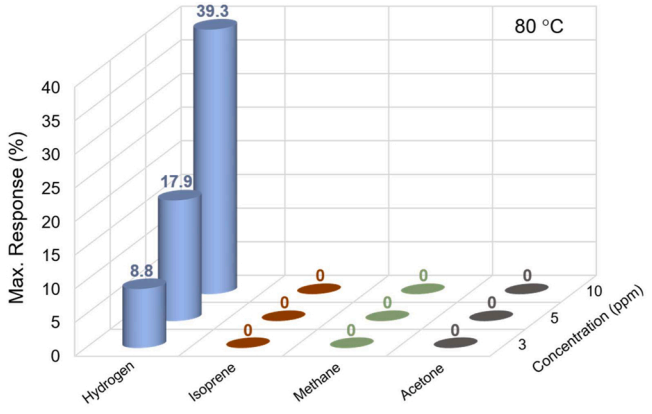

Fig. 12. Selectivity test of the dual-channel H_2 gas sensor: maximum sensing response for 3, 5, and 10 ppm of H_2 and other gases at 80 °C.

measurements. The long-term stability was tested by sensing measurements at H_2 concentrations of 50 and 300 ppm for 76 days at random intervals. The base resistance in air (Fig. 10(a)) and change in sensing resistance to H_2 exposure (Fig. 10(b)) were found to be nearly constant over 76 days. These results indicate that the dual-channel Pd-coated SnO_2 NR sensor has excellent and reliable performance for H_2 detection.

We further tested the effect of humidity on the dual-channel sensor for different concentrations of H_2 at 80 °C. Fig. 11 shows the resistance variation with time for 500- and 10-ppm H_2 under different humidities (0–90 RH%). For the high concentration of H_2 (500 ppm), the resistance change was almost constant even under high humidity. However, the sensor response decreased significantly with increasing humidity for a low concentration of H_2 (10 ppm). This is because more water molecules are adsorbed on the surface of the sensing material under high humidity, resulting in a significant reduction in the number of reaction sites for detection of the target gas. Furthermore, the selectivity test was performed for 3-, 5-, and 10-ppm H_2 and other gases (isoprene, methane, and acetone) at 80 °C. As shown in Fig. 12, the dual-channel Pd-coated SnO_2 senor exhibited remarkably high selectivity for H_2 detection. This is because the sensing reaction of heavier molecules such as isoprene, methane, and acetone is significantly suppressed at the low operating temperature of 80 °C.

The detailed mechanism for the lower sensing temperature of the dual-channel sensors compared with the conventional ones can be explained by hydrogen partial desorption, as shown in Fig. 13. At a low temperature (below 100 °C), oxygen molecules in air atmosphere are simply physisorbed on the surface of SnO_2 [20,38,52]. However, the oxygen ion species are easily adsorbed over the surface of Pd NPs by attracting electrons from SnO_2. Because of the spillover effect of Pd NPs, oxygen ions spread out on the surface of SnO_2. These cause the formation of a thick electron-depletion layer on the surface of SnO_2. Consequently, the resistance of Pd-coated SnO_2 NPs ($R_{ch.1}$) increases, which is much higher than the resistance of the secondary conduction channel through the electrode/substrate ($R_{ch.2}$). The current mainly flows through the interface at Cr/native oxide/p-type Si and p-type Si ($R_{ch.2}$) (Fig. 13(a)). When the dual-channel sensor is exposed to H_2/air, the chemisorbed oxygen ion species react with H_2 to form H_2O. In this process, electrons are released and returned to SnO_2, resulting in the reduction in the thickness of the depletion region. This reaction makes the conductance of SnO_2 NRs higher than that of the second channel, so that the main current flows through the SnO_2 NRs ($R_{ch.1}$), as shown in Fig. 13(b).

Notably, a temperature below 100 °C is not high enough to fully recover the initial surface state of the Pd-SnO_2 NRs in the H_2 out cycle, resulting in incomplete recovery of the baseline resistance, which causes the problem of slow and irreversible change in the case of a conventional single-channel sensor. However, in the case of the dual-channel sensor, the second conduction channel with $R_{ch.2}$, which is more stable, becomes the main conduction path in air. Although the first conduction path with $R_{ch.1}$ is not fully recovered, a highly stable and reversible hydrogen response/recovery signal can be obtained and persists at temperatures below 100 °C. This switching mechanism can also be explained by $R_{ch.1}$ and $R_{ch.2}$ operating in parallel ($1/R_{total} = 1/R_{ch.1} + 1/R_{ch.2}$). Accordingly, we demonstrated the highly stable and reversible hydrogen sensors, which could operate at temperatures below 100 °C.

One notable point is that in this study the optimal baseline resistance of the sensor was achieved through the Cr/native oxide/Si hybrid Schottky barrier. Moreover, we expect that a higher baseline resistance (a higher barrier height) is needed to achieve optimum performance for sensing heavy gas molecules at higher temperatures. Investigating alternative materials or fabrication processes for providing optimal Schottky barrier height and the resistance of the second channel is also important. Accordingly, the concept of the dual-channel sensors utilizing the interface between the metal electrode and Si substrate can be generally employed for detection of various types of gases in a controlled manner. This work paves the way for improving gas-sensing performance through interface engineering, enabling practical sensor applications.

4. Conclusion

We present a highly stable and reversible H_2 sensor that operates with a dual electron-conduction channel comprising a sensing material (Pd-coated SnO_2 NRs) channel ($R_{ch.1}$) and a parallel conduction channel ($R_{ch.2}$) with electrode/substrate interface and substrate. TEM analysis revealed sharp interfaces between the Cr layer and p-type Si, with a 1.7-

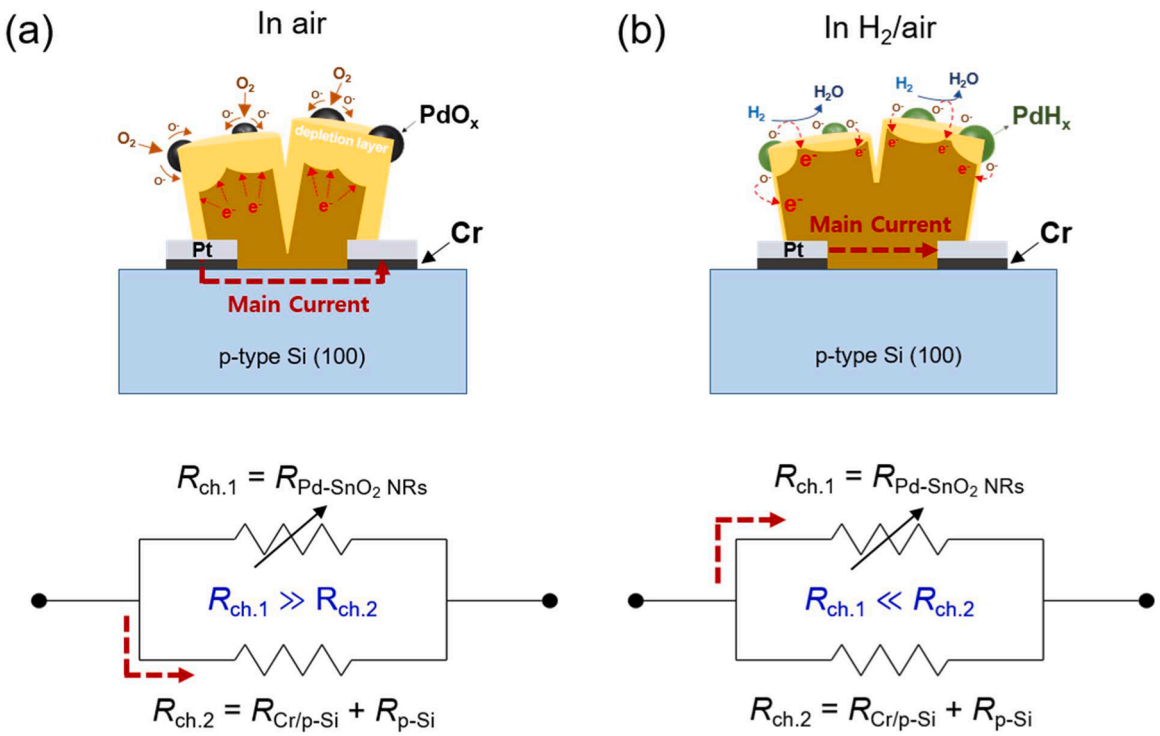

Fig. 13. Schematics showing the sensing mechanism in dual-channel H_2 gas sensors. (a) In air, oxygen is adsorbed on the Pd surface and electrons at SnO_2 are attracted to the surface, resulting in widening of the depletion layer (high-resistance state of Pd-coated SnO_2 NRs). In this case, the interface at Cr/p-type Si and p-type Si itself serves as the main conduction channel. (b) Under H_2 gas exposure, the surface oxygen can be removed, and then the depletion layer is reduced (low-resistance state of Pd-coated SnO_2 NRs), so that Pd-SnO_2 NRs act as the main conduction channel.

nm-thick native oxide layer existing between them. By using an electrically conductive p-type Si substrate ($R_{p\text{-}Si}$) instead of insulating SiO_2 (300 nm)/Si substrate and utilizing a Cr/native oxide/p-type Si interface as a Schottky barrier ($R_{Cr/p\text{-}Si}$), a parallel conduction channel ($R_{ch.2} = R_{Cr/p\text{-}Si} + R_{p\text{-}Si}$) was formed. Therefore, the dual channel sensor works with a parallel resistor model ($1/R_{total} = 1/R_{ch.1} + 1/R_{ch.2}$). In air atmosphere, $R_{ch.1}$ is much higher than $R_{ch.2}$. Thus, when the sensor is in air, the current mainly flows through the interface of Cr/p-type Si and p-type Si, thereby keeping the base resistance stable at $R_{ch.2}$. Under H_2 exposure, $R_{ch.1}$ becomes much lower than $R_{ch.2}$ owing to the H_2-sensing reaction. Because of this switching mechanism, the dual-channel sensor exhibited highly reversible resistance changes during H_2 in-and-out cycles at operating temperatures of 25 °C– 100 °C. The dual-channel Pd-coated SnO_2 NR sensor showed excellent performance in terms of reproducibility, long-term stability, and selectivity in H_2 sensing at 80 °C, which enables practical H_2 sensor applications. In addition, by using this sensor, H_2 at 1% or more could be detected within 2 s, and the sensing response for H_2 at 500 ppm or more could be stably obtained without interference form high humidity. Moreover, the sensor was able to detect H_2 below 0.5 ppm. This work provides a route to improve gas-sensing performance through interface engineering, enabling a variety of practical hydrogen sensor applications, such as hydrogen leak detectors and hydrogen breath analyzer.

CRediT authorship contribution statement

Jinkyo Jeong: Conceptualization, Investigation, Visualization, Writing – original draft. **Jung-Woo Lee**: Validation, Visualization, **Jaeung Lee**: Investigation, Visualization, **Kyusik Shin:** Validation, Visualization, **Hyun-Sook Lee:** Conceptualization, Validation, Writing – original draft, Writing – review & editing preparation. **Wooyoung Lee:** Supervision.

Declaration of Competing Interest

The authors declare that they have no known competing financial interests or personal relationships that could have appeared to influence the work reported in this paper.

Data Availability

Data will be made available on request.

Acknowledgement

This research was supported by the National Research Foundation of Korea (NRF) grant funded by the Korea government (MIST) (No. NRF-2022M3H4A3053304, National Core Materials Research Center (Platform type) and by the Technology Innovation Program (‘20013621’, Center for Super Critical Material Industrial Technology) funded by the Ministry of Trade, Industry & Energy (MOTIE, Korea). This research was also supported by the Basic Science Research Program through the National Research Foundation of Korea (NRF) funded by the Ministry of Education (NRF-2019R1A6A1A11055660). H.-S. Lee gratefully acknowledges the support from the Basic Research in Science and Engineering Program of the NRF (2021R1A2C1013690). J. -W. Lee gratefully acknowledges the support from the Korea Initiative for fostering the University of Research and Innovation (KIURI) Program of the NRF (2020M3H1A1077207).

Appendix A. Supporting information

Supplementary data associated with this article can be found in the online version at doi:10.1016/j.snb.2023.134350.

References

[1] V.A. Goltsov, T.N. Veziroglu, A step on the road to hydrogen civilization, Int. J. Hydrog. Energy 27 (2002) 719–723.
[2] P. Liu, X. Han, Comparative analysis on similarities and differences of hydrogen energy development in the World's top 4 largest economies: a novel framework, Int. J. Hydrog. Energy 47 (2022) 9485–9503.
[3] D.A. Crowl, Y.D. Jo, The hazards and risks of hydrogen, J. Loss Prev. Process Ind. 20 (2007) 158–164.
[4] W.J. Buttner, M.B. Post, R. Burgess, C. Rivkin, An overview of hydrogen safety sensors and requirements, Int. J. Hydrog. Energy 36 (2011) 2462–2470.
[5] H.C. Sun, Y.C. Huang, C.M. Huang, A review of dissolved gas analysis in power transformers, Energy Procedia 14 (2012) 1220–1225.
[6] D. Li, J.W. Medlin, R. Bastasz, Application of polymer-coated metal-insulator-semiconductor sensors for the detection of dissolved hydrogen, Appl. Phys. Lett. 88 (2006), 233507.
[7] F. Yang, D. Jung, R.M. Penner, Trace detection of dissolved hydrogen gas in oil using a palladium nanowire array, Anal. Chem. 83 (2011) 9472–9477.
[8] B. Jang, M.H. Kim, J. Baek, W. Kim, W. Lee, Highly sensitive hydrogen sensors: Pd-coated Si nanowire arrays for detection of dissolved hydrogen in oil, Sens. Actuators, B 273 (2018) 809–814.
[9] M.H. Kim, B. Jang, W. Kim, W. Lee, Enhanced hydrogen sensing properties of Pd-coated SnO_2 nanorod arrays in nitrogen and transformer oil, Sens. Actuators, B 283 (2019) 890–896.
[10] L. Pauling, A.B. Robinson, R. Teranishi, P. Cary, Quantitative analysis of urine vapor and breath by gas-liquid partition chromatography, Proc. Natl. Acad. Sci. U. S. A 68 (1971) 2374–2376.
[11] A. Eisenmann, A. Amann, M. Said, B. Datta, M. Ledochowski, Implementation and interpretation of hydrogen breath tests, J. Breath. Res. 2 (2008), 046002.
[12] W. Shin, Medical applications of breath hydrogen measurements, Anal. Bioanal. Chem. 406 (2014) 3931–3939.
[13] L. Boon-Brett, J. Bousek, G. Black, P. Moretto, P. Castello, T. Hübert, U. Banach, Identifying performance gaps in hydrogen safety sensor technology for automotive and stationary applications, Int. J. Hydrog. Energy 35 (2010) 373–384.
[14] T. Hübert, L. Boon-Brett, G. Black, U. Banach, Hydrogen sensors–a review, Sens. Actuators, B 157 (2011) 329–352.
[15] L. Boon-Brett, J. Bousek, P. Moretto, Reliability of commercially available hydrogen sensors for detection of hydrogen at critical concentrations: part ii–selected sensor test results, Int. J. Hydrog. Energy 34 (2009) 562–571.
[16] N. Yamazoe, New approaches for improving semiconductor gas sensors, Sens. Actuators, B 5 (1991) 7–19.
[17] Y. Luo, C. Zhang, B. Zheng, X. Geng, M. Debliquy, Hydrogen sensors based on noble metal doped metal-oxide semiconductor: a review, Int. J. Hydrog. Energy 42 (2017) 20386–20397.
[18] G. Korotcenkov, Gas response control through structural and chemical modification of metal oxide films: state of the art and approaches, Sens. Actuators, B 107 (2005) 209–232.
[19] N. Yamazoe, K. Shimanoe, Proposal of contact potential promoted oxide semiconductor gas sensor, Sens. Actuators, B 187 (2013) 162–167.
[20] G.J. Li, X.H. Zhang, S. Kawi, Relationships between sensitivity, catalytic activity, and surface areas of SnO_2 gas sensors, Sens. Actuators, B 60 (1999) 64–70.
[21] S. Das, V. Jayaraman, SnO_2: a comprehensive review on structures and gas sensors, Prog. Mater. Sci. 66 (2014) 112–255.
[22] N. Barsan, M. Schwerizer-Berberich, W. Göpel, Fundamental and practical aspects in the design of nanoscaled SnO_2 gas sensors: a status report, Fresenius' J. Anal. Chem. 365 (1999) 287–304.
[23] J. Zhao, W. Wang, Y. Liu, J. Ma, X. Li, Y. Du, G. Lu, Ordered mesoporous Pd/SnO_2 synthesized by a nanocasting route for high hydrogen sensing performance, Sens. Actuators, B 160 (2011) 604–608.
[24] G. Singh, Virval, R.C. Singh, Highly sensitive gas sensor based on Er-doped SnO_2 nanostructures and its temperature dependent selectivity towards hydrogen and ethanol, Sens. Actuators, B 282 (2019) 373–383.
[25] M. Kooti, S. Keshtkar, M. Askarieh, A. Rashidi, Progress toward a novel methane gas sensor based on SnO_2 nanorods-nanoporous graphene hybrid, Sens. Actuators, B 281 (2019) 96–106.
[26] F. Fan, J. Zhang, J. Li, N. Zhang, R. Hong, X. Deng, P. Tang, D. Li, Hydrogen sensing properties of Pt-Au bimetallic nanoparticles loaded on ZnO nanorods, Sens. Actuators, B 241 (2017) 895–903.
[27] N. Tamaekong, C. Liewhiran, A. Wisitsoraat, S. Phanichphant, Sensing characteristics of flame-spray-made Pt/ZnO thick films as H_2 gas sensor, Sensors 9 (2009) 6652–6669.
[28] Q.A. Drmosh, Z.H. Yamani, Hydrogen sensing properties of sputtered ZnO films decorated with Pt nanoparticles, Ceram. Int. 42 (2016) 12378–12384.
[29] S. Joo, I. Muto, Nobuyoshi Hara, Hydrogen gas sensor using Pt-and Pd-added anodic TiO_2 nanotube films, J. Electrochem. Soc. 157 (2010) J221–J226.
[30] A. Esfandiar, S. Ghasemi, A. Irajizad, O. Akhavan, M.R. Gholami, The decoration of TiO_2/reduced graphene oxide by Pd and Pt nanoparticles for hydrogen gas sensing, Int. J. Hydrog. Energy 37 (2021) 15423–15432.
[31] J. Moon, H.P. Hedman, M. Kemell, A. Tuominen, R. Punkkinen, Hydrogen sensor of Pd-decorated tubular TiO_2 layer prepared by anodization with patterned electrodes on SiO_2/Si substrate, Sens. Actuators, B 222 (2016) 190–197.
[32] Y.-S. Shim, B. Jang, J.M. Suh, M.S. Noh, S. Kim, S.D. Han, Y.G. Song, D.H. Kim, C.-Y. Kang, H.W. Jang, W. Lee, Nanogap-controlled Pd coating for hydrogen sensitive switches and hydrogen sensors, Sens. Actuators B Chem. 255 (2018) 1841–1848.
[33] S. Hwan Cho, J. Min Suh, B. Jeong, T. Hyung Lee, K. Soon Choi, T. Hoon Eom, T. Kim, H. Won Jang, Fast responding and highly reversible gasochromic H_2 sensor using pd-decorated amorphous WO_3 thin films, Chem. Eng. J. 446 (2022), 136862.
[34] S.K. Arya, S. Krishnan, H. Silva, S. Jean, S. Bhansali, Advances in materials for room temperature hydrogen sensors, Analyst 137 (2012) 2743–2756.
[35] M. Kumar, R. Kumar, S. Rajamani, S. Ranwa, M. Fanetti, M. Valant, M. Kumar, Efficient room temperature hydrogen sensor based on UV-activated ZnO nano-network, Nanotechnology 28 (2017), 365502.
[36] G. Liu, Z. Wang, Z. Chen, S. Yang, X. Fu, R. Huang, X. Li, J. Xiong, Y. Hu, H. Gu, Remarkably enhanced room-temperature hydrogen sensing of SnO_2 nanoflowers via vacuum annealing treatment, Sensors 18 (2018) 949.
[37] I.H. Kadhim, H.A. Hassan, Q.N. Abdullah, Hydrogen gas sensor based on nanocrystalline SnO_2 thin film grown on bare Si substrates, Nano-Micro Lett. 8 (2016) 20–28.
[38] T. Lei, Z. Rao, S. Zhang, S. Cai, C. Xie, The irreversible RT curves of metal oxide gas sensor under programmed temperature cycle, Sens. Actuators, B 235 (2016) 481–491.
[39] B.I. Armitage, K. Murugappan, M.J. Lefferts, A. Cowsik, M.R. Castell, Conducting polymer percolation gas sensor on a flexible substrate, J. Mater. Chem. C. 8 (2020) 12669–12676.
[40] J.H. Lee, A. Katoch, S.W. Choi, J.H. Kim, H.W. Kim, S.S. Kim, Extraordinary improvement of gas-sensing performances in SnO_2 nanofibers due to creation of local p–n heterojunctions by loading reduced graphene oxide nanosheets, ACS Appl. Mater. Interfaces 7 (2015) 3101–3109.
[41] V. Van Quang, N. Van Dung, N.S. Trong, N.D. Hoa, N. Van Duy, N. Van Hieu, Outstanding gas-sensing performance of graphene/SnO_2 nanowire Schottky junctions, Appl. Phys. Lett. 105 (2014), 013107.
[42] G. Bae, I.S. Jeon, M. Jang, W. Song, S. Myung, J. Lim, S.S. Lee, H.K. Jung, C. Y. Park, K.S. An, Complementary dual-channel gas sensor devices based on a role-allocated ZnO/graphene hybrid heterostructure, ACS Appl. Mater. Interfaces 11 (2019) 16830–16837.
[43] Y. Peng, L. Zheng, K. Zou, C. Li, Enhancing performances of a resistivity-type hydrogen sensor based on Pd/SnO_2/RGO nanocomposites, Nanotechnology 28 (2017), 215501.
[44] R.T. Tung, The physics and chemistry of the Schottky barrier height, Appl. Phys. Rev. 1 (2014), 011304.
[45] T. Kilicoglu, S. Asubay, The effect of native oxide layer on some electronic parameters of Au/n-Si/Au–Sb Schottky barrier diodes, Phys. B 369 (2005) 58–63.
[46] Z. Caldiran, Modification of Schottky barrier height using an inorganic compound interface layer for various contact metals in the metal/p-Si device structure, J. Alloy. Compd. 865 (2021), 158856.
[47] I. Bondarchuk, F.J. Cadete Santos Aires, G. Mamontov, I. Kurzina, Preparation and Investigation of Pd and Bimetallic Pd-Sn Nanocrystals on γ-Al2O3, Crystals 11 (2021) 444.
[48] K.D. Schierbaum, U.K. Kirner, J.F. Geiger, W. Göpel, Schottky-barrier and conductivity gas sensors based upon Pd/SnO_2 and Pt/TiO_2, Sens. Actuators, B 4 (1991) 87–94.
[49] B.L. Smith, E.H. Rhoderick, Schottky Barriers on p-type silicon, Solid-State Electron 14 (1971) 71–75.
[50] N.M. Vuong, D. Kim, H. Kim, Surface gas sensing kinetics of a WO_3 nanowire sensor: Part 2—Reducing gases, Sens. Actuators, B 224 (2016) 425–433.
[51] F. Gui, Y. Huang, M. Wu, X. Lu, Y. Hu, W. Chen, Aging behavior and heat treatment for room-temperature CO-sensitive Pd-SnO_2 composite nanoceramics, Materials 15 (2022) 1367.
[52] J.E. Lennard-Jones, Processes of adsorption and diffusion on solid surfaces, Trans. Faraday Soc. 28 (1932) 333–359.

Jinkyo Jeong received his Master's degree in Vehicle Convergence Engineering at Yonsei University in 2023. He studied metal oxide-based materials and semiconductor device processes for hydrogen gas sensor under the supervision of Prof. Wooyoung Lee.

Jung-Woo Lee is currently an assistant professor in the Department of Materials Science and Engineering at Hongik University in Sejong, Korea. He received a Ph.D. degree in Materials Science and Engineering at Seoul National University in 2013. He had worked as a research associate and assistant scientist at University of Wisconsin-Madison from 2014 to 2021. Since 2021, he had worked as a research professor in KIURI (Korea Initiative for fostering University of Research & Innovation) institute at Yonsei University. His research interests are synthesis and characterization of functional complex thin films.

Kyusik Shin is currently a research professor in Center for Super Critical Material Industrial Technology, the Department of Materials Science and Engineering at Yonsei University, Seoul, Korea. He received a Ph.D. degree in Materials Science from University of Minnesota, Twin Cities, United States in 1995. His research interests are on nanostructured metal oxide semiconductor gas sensors, breath analysis, hard magnets, and magnetic sensor materials.

Hyun-Sook Lee received a Ph.D. degree in Physics at POSTECH in 2008. Since 2015, she has been working as a research professor in the Department of Materials Science and Engineering at Yonsei University. Her research interests are in various materials related to high-temperature superconductors, solid-state hydrogen storages, rare-earth/rare-earth-free permanent magnets, nanostructured metal oxide semiconductor gas sensors, and Pd-based hydrogen sensors.

Wooyoung Lee is a professor of the Department of Materials Science and Engineering and the Director of Center for Super Critical Material Industrial Technology (MOTIE) at Yonsei University in Korea. He received a BS degree in Metallurgical Engineering in 1986, a MS degree in Metallurgical Engineering from the Yonsei University in 1988. He received a Ph. D. degree in Physics from University of Cambridge, United Kingdom in 2000. He is a regular member of National Academy of Engineering of Korea. He was a member of National Science & Technology Council and a director in Korea Israel Industrial R&D Foundation. In recent years, his research interests have centered on hydrogen sensors, various metal oxide semiconducting gas sensors, and breath analyzers. He is also studying thermoelectric materials and devices, and permanent magnets. He has received a number of awards in nano-related research areas and a Service Merit Medal (2008) from the Government of Korea due to contribution on the development of intellectual properties. He has authored and co-authored over 200 publications, and has edited three special books on nano-structured materials and devices.